Acta Crystallographica Section F
Structural Biology and Crystallization Communications
ISSN 1744-3091

Crystallization and preliminary X-ray diffraction analysis of the N-terminal domain of Mrs2, a magnesium ion transporter from yeast inner mitochondrial membrane

Muhammad Bashir Khan,[a] Björn Sjöblom,[a] Rudolf J. Schweyen[b]† and Kristina Djinović-Carugo[a,c]*

[a]Department for Structural and Computational Biology, Max F. Perutz Laboratories, University of Vienna, Vienna, Austria, [b]Department of Microbiology, Immunobiology and Genetics, Max F. Perutz Laboratories, University of Vienna, Vienna, Austria, and [c]Department of Biochemistry, Faculty of Chemistry and Chemical Technology, University of Ljubljana, Ljubljana, Slovenia

† Deceased February 2009.

Correspondence e-mail: kristina.djinovic@univie.ac.at

Received 18 February 2010
Accepted 31 March 2010

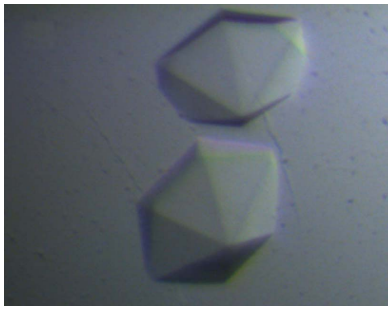

Mrs2 transporters are distantly related to the major bacterial Mg^{2+} transporter CorA and to Alr1, which is found in the plasma membranes of lower eukaryotes. Common features of all Mrs2 proteins are the presence of an N-terminal soluble domain followed by two adjacent transmembrane helices (TM1 and TM2) near the C-terminus and of the highly conserved F/Y-G-M-N sequence motif at the end of TM1. The inner mitochondrial domain of the Mrs2 from *Saccharomyces cerevisae* was overexpressed, purified and crystallized in two different crystal forms corresponding to an orthorhombic and a hexagonal space group. The crystals diffracted X-rays to 1.83 and 4.16 Å resolution, respectively. Matthews volume calculations suggested the presence of one molecule per asymmetric unit in the orthorhombic crystal form and of five or six molecules per asymmetric unit in the hexagonal crystal form. The phase problem was solved for the orthorhombic form by a single-wavelength anomalous dispersion experiment exploiting the sulfur anomalous signal.

1. Introduction

Mg^{2+} is the most abundant divalent cation in cells and organelles (Diwan, 1987). It plays important roles in stabilizing macromolecules and in binding to nucleotides and acts as a cofactor of many enzymes. By regulating the activities of ion channels and transporters, Mg^{2+} also influences cell volume and signalling processes (Ikari *et al.*, 2008; Mobasheri *et al.*, 1998).

Mrs2 transporters form the major mitochondrial Mg^{2+}-uptake system in yeast, plants and mammals (Zsurka *et al.*, 2001; Kolisek *et al.*, 2003; Li *et al.*, 2001; Schock *et al.*, 2000) and are essential for mitochondrial biogenesis (Walker *et al.*, 1982). Mrs2 transporters are distantly related to the major bacterial Mg^{2+} transporter CorA and to Alr1, which is located in the plasma membrane of lower eukaryotes. The amino-acid sequence identity between the N-terminal domains of CorA from *Thermotoga maritima* and Mrs2 from *Saccharomyces cerevisae* is 11%. The members of the Alr1 subfamily appear to be restricted to lower eukaryotes, where they form the major Mg^{2+}-uptake system of the plasma membrane. Expression of Alr1 is essential for the growth of yeast cells, except when kept in media with nonphysiologically high Mg^{2+} concentrations (Graschopf *et al.*, 2001). On the other hand, the cellular uptake of Mg^{2+} in mammals is mediated by proteins unrelated to the CorA–Mrs2–Alr1 superfamily that belong to the mammalian melastatin-related transient receptor potential (TRPM) family of cation channels (TRPM6 and TRPM7; Voets *et al.*, 2004; Schmitz *et al.*, 2005).

Common features of all of these proteins are the presence of two adjacent transmembrane helices (TM1 and TM2) near the C-terminus and of the highly conserved F/Y-G-M-N sequence motif at the C-terminus of TM1 (Bui *et al.*, 1999; Gardner, 2003; Knoop *et al.*, 2005; Lunin *et al.*, 2006). The N-terminus is characterized by a large cytoplasmic domain which forms a funnel and has been shown to constitute an allosteric regulatory module that can be engineered to promote an activated or closed state (Payandeh *et al.*, 2008).

Despite low amino-acid sequence identity, secondary-structure features appear to be conserved in the N-terminal and transmembrane portions of all members of the CorA–Mrs2–Alr1 superfamily (Lunin *et al.*, 2006), while they display notable differences in the

region C-terminal to TM2 (Gardner, 2003). Moreover, some of these transporters can partially replace each other, which strongly supports the notion that they are orthologues (Bui *et al.*, 1999; Lunin *et al.*, 2006; Li *et al.*, 2001; R. Schweyen, unpublished work).

Mrs2 is located in the inner mitochondrial membrane, while Alr1 is inserted into the cytoplasmic membrane. The orientation of these transporters in their cognate membranes is such that both the long sequence N-terminal to TM1 and the sequences C-terminal to TM2 are oriented towards the mitochondrial matrix and the cytoplasm in Mrs2 and Alr1, respectively. Only a short loop connecting the TM helices is oriented towards the space between the two mitochondrial membranes and outside in Mrs2 and Alr1, respectively (Baumann *et al.*, 2002; Bui *et al.*, 1999; Wachek *et al.*, 2006). In their cognate membranes yeast Mrs2 and Alr1 have been shown to form homo-oligomers, while the bacterial transporter CorA was found to be in a pentameric state (Kolisek *et al.*, 2003; Wachek *et al.*, 2006; Warren *et al.*, 2004; Weghuber *et al.*, 2006).

Here, we report the crystallization and X-ray diffraction analysis of the N-terminal domain of Mrs2, the Mg^{2+} transporter from yeast inner mitochondrial membrane.

2. Materials and methods

2.1. Cloning and expression

The gene encoding the mitochondrial magnesium transporter Mrs2 (YOR334W) from *S. cerevisae* was used to amplify the mitochondrial matrix domain of Mrs2 ($Mrs2_{16–276}$; M_r = 30 124) by polymerase chain reaction (PCR) using *Taq* DNA polymerase with the forward primer 5′-CTTTATTTTCAGGGCG**CCATGG**GCAAACAGTTACTATC-GTTGAAGCCCATT-3′ and the reverse primer 5′-GTGCTCGAGT-**GCGGCCGC**TTATAAGGAATTTCTATTTGCGTCCAATATGA-T-3′, which were designed based on the nucleotide sequence of the Mrs2 gene. The PCR product was digested with *Nco*I and *Not*I (the recognition sites are shown in bold in the primers used) and cloned into the vector pETM-11 (EMBL Hamburg) with a tobacco etch virus (TEV) cleavable N-terminal His_6 tag MKHHHHHHPMSDYDIPT-TENLYFQGA. The DNA insert cloned in pETM-11 was sequenced to confirm the fidelity of DNA amplification.

The recombinant protein was overexpressed in BL-21 Star (DE3) *Escherichia coli* transformants grown in LB medium containing kanamycin (0.025 mg ml^{-1}) at 310 K with shaking at 200 rev min^{-1}; the cells were induced at an OD_{600} of 0.6 with 0.5 m*M* isopropyl β-D-1-thiogalactopyranoside (IPTG) and allowed to grow to a final OD_{600} of 2.3 at 294 K. The cells were harvested by centrifugation (6000*g*, 30 min), resuspended in sonication buffer (50 m*M* Tris–HCl pH 8.0, 500 m*M* NaCl) supplemented with 1 m*M* phenylmethanesulfonyl-fluoride (PMSF), 5 m*M* β-mercaptoethanol (BME), 20 m*M* imidazole and 5% glycerol, and lysed by sonication.

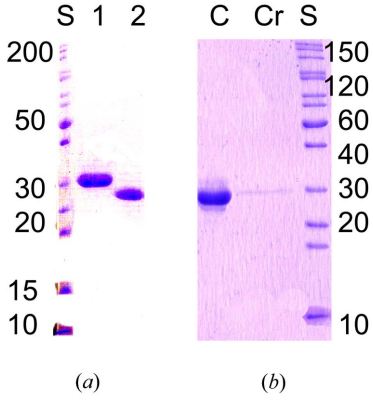

Figure 1
SDS–PAGE gels of TEV cleavage of $Mrs2_{16–276}$ and of dissolved $Mrs2_{16–276}$ crystals (form *A*). (*a*) Lane 1, before His_6-tag cleavage; lane 2, after His_6-tag cleavage with TEV; lane S, molecular-weight standards (kDa). (*b*) Lane C, control; lane Cr, dissolved crystals; lane S, molecular-weight standards (kDa).

2.2. Purification

After sonication of the cells, the crude extract was centrifuged at 50 000*g* for 30 min and the supernatant was loaded onto a 5 ml Ni–NTA agarose column (Qiagen) pre-equilibrated in buffer *A* (50 m*M* Tris–HCl pH 8.0, 500 m*M* NaCl, 1 m*M* PMSF, 5 m*M* BME, 20 m*M* imidazole and 5% glycerol). The column was extensively washed with buffer *A* containing 20 m*M* imidazole. The protein was eluted with a linear gradient of buffer *B* containing 500 m*M* imidazole. The N-terminal His_6 tag was cleaved using TEV (protease:protein mass ratio 1:70) for 12 h during dialysis against 50 m*M* Tris–HCl pH 8.0 containing 300 m*M* NaCl, 1 m*M* dithiothreitol (DTT) and 1 m*M* PMSF. The cleaved N-terminus and TEV were separated from the protein after TEV cleavage by again applying the reaction mixture onto the Ni–NTA column. The flowthrough was pooled and loaded onto a Resource Q column (6 ml; GE Healthcare) equilibrated with buffer *A* consisting of 50 m*M* Tris–HCl pH 8.0, 20 m*M* NaCl, 5 m*M* BME and 1 m*M* PMSF and the protein was eluted using a gradient of 20–1000 m*M* NaCl in 50 m*M* Tris–HCl pH 8.0, 5 m*M* BME and 1 m*M* PMSF. The protein eluted from the Resource Q column in a single peak at 280 m*M* NaCl. Further purification was carried out on a HiLoad 26/60 Superdex 200 (GE Healthcare) gel-filtration column in 50 m*M* Tris–HCl pH 8.0 and 300 m*M* NaCl. The protein eluted in a single peak at an elution volume of 218 ml, corresponding to a molecular weight of 30 kDa, which is compatible with the monomer of $Mrs2_{16–276}$. The purified protein was concentrated by reapplying it onto a Resource Q column (6 ml; GE Healthcare) as described above; it was concentrated to about 3 mg ml^{-1} for crystallization screening. These procedures reproducibly yielded 6 mg protein from 1 l of bacterial culture.

The purity of the protein solution used in the crystallization experiments was checked by SDS–PAGE analysis and showed a single band with an apparent molecular weight of about 30 kDa (Fig. 1*a*).

Dynamic light scattering was used to assess the monodispersity of the protein solution: a monomodal distribution with a polydispersity of 5% was observed and the gyration radius was estimated to be 4.2 nm, suggesting that the protein solution was homogenous and monomeric. Circular-dichroism spectroscopy in the far-ultraviolet wavelength range showed that the protein was rich in α-helical content.

2.3. Crystallization

Initial screening for crystallization conditions was performed using Crystal Screens 1 and 2, PEG/Ion Screen, Index, Natrix, SaltRX, Cryo 1 and 2, JCSG, PACT and MembFac kits from Hampton Research. A nanodrop crystallization robot (Phoenix RE, Matrix Technologies) was employed for screening using the sitting-drop vapour-diffusion method at 295 K, mixing equal volumes (0.2 µl) of protein solution (3 mg ml^{-1} in anion-exchange buffer) and reservoir solution. Crystals of $Mrs2_{16–276}$ were initially obtained from Cryo 1 and 2 condition No. 59, consisting of 0.1 *M* sodium/potassium phosphate pH 6.2, 25%(*v*/*v*) 1,2-propanediol, 10%(*v*/*v*) glycerol, and condition No. 22, composed of 0.1 *M* sodium/potassium phosphate pH 6.2, 40%(*v*/*v*) ethylene glycol. For optimization of crystallization

conditions, 1 µl protein solution (3 mg ml^{-1} in anion-exchange buffer) was mixed with 1 µl mother liquor for vapour-diffusion experiments against 0.5 ml reservoir solution. After further optimization of the crystallization conditions, the best crystals were obtained using 22%(*v*/*v*) ethylene glycol, 56 m*M* sodium/potassium phosphate pH 6.3. The crystals (form *A*) appeared overnight and grew to maximum dimensions of about 0.5 × 0.2 × 0.2 mm within 2–3 d (Fig. 2*a*). Small crystals of Mrs2$_{16–276}$ (form *B*) were also obtained in the presence of 1.7 *M* NaCl, 70 m*M* imidazole pH 7.8 at 295 K (Fig. 2*b*). However, these crystals did not diffract to high resolution.

The crystals (form *A*) were dissolved in deionized water at room temperature. SDS–PAGE was performed on 12.5% polyacrylamide. The protein bands of dissolved crystals were identified by comparing their mobility with those of protein standard molecular-weight markers and purified Mrs2$_{16–276}$ (Fig. 1*b*).

2.4. X-ray diffraction

All Mrs2$_{16–276}$ X-ray diffraction data sets were collected at 100 K in a cold nitrogen stream using either an in-house Bruker Microstar

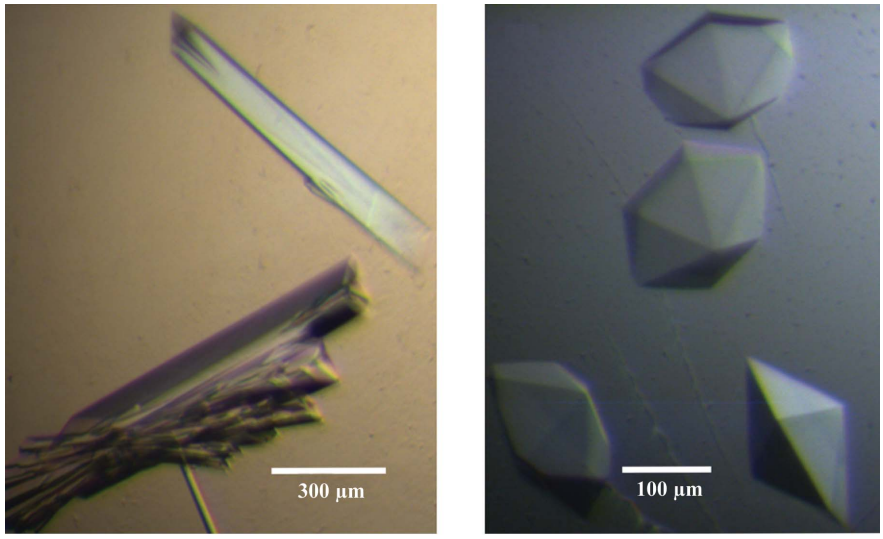

(*a*) (*b*)

Figure 2
The two different forms of Mrs2$_{16–276}$ crystals. (*a*) Crystals of Mrs2$_{16–276}$ grown in 22%(*v*/*v*) ethylene glycol, 56 m*M* sodium/potassium phosphate pH 6.3 (form *A*). (*b*) Crystals of Mrs2$_{16–276}$ grown in 1.7 *M* NaCl, 70 m*M* imidazole pH 7.8 (form *B*).

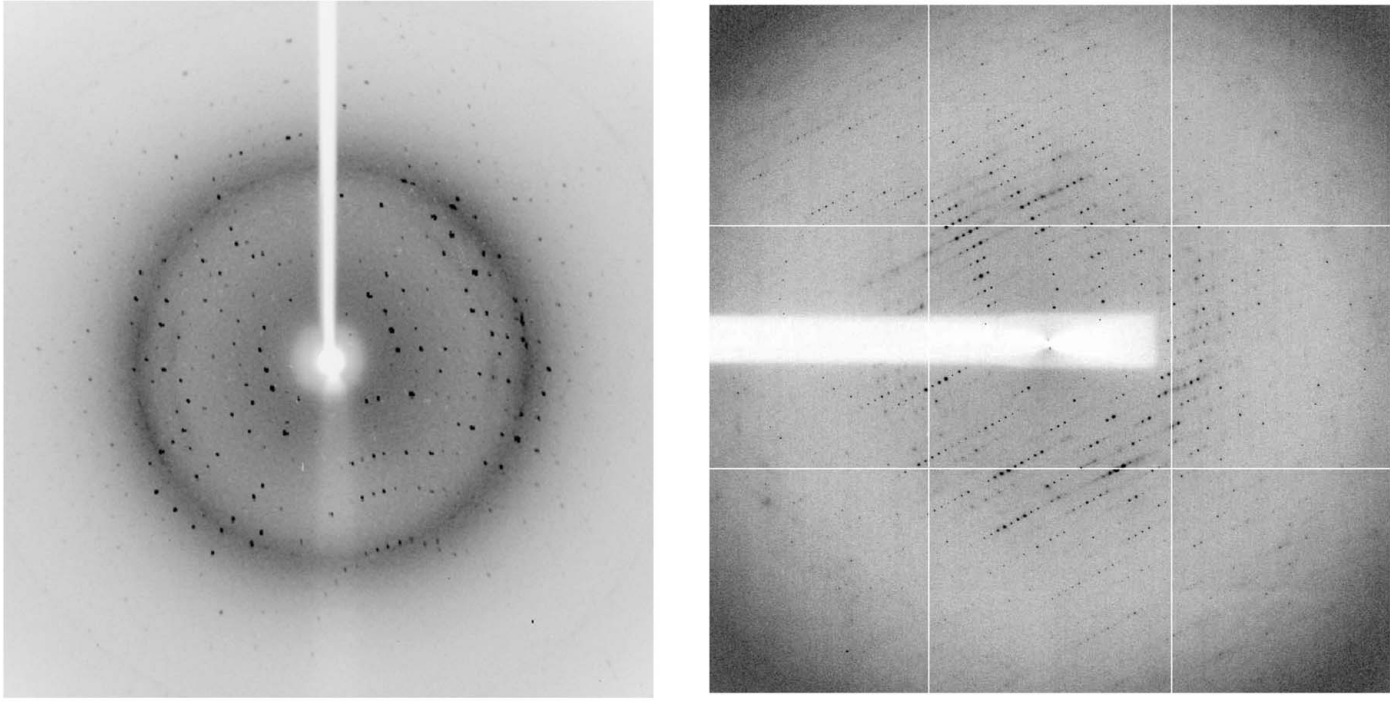

(*a*) (*b*)

Figure 3
Diffraction patterns of Mrs2$_{16–276}$ crystals. (*a*) Diffraction pattern of form *A* Mrs2$_{16–276}$ crystals. The resolution is ∼1.8 Å at the edge. (*b*) Diffraction pattern of form *B* Mrs2$_{16–276}$ crystals. The resolution is ∼3.4 Å at the edge.

Table 1
Data-collection statistics for the N-terminal domain of Mrs2.

Values in parentheses are for the outermost resolution shell. No $\sigma(I)$ cutoff was used in the data-integration process.

	Form *A* (home source)	Form *B* (ESRF ID14-1)
Wavelength (Å)	1.54178	0.933
Temperature (K)	100	100
Space group	$P2_12_12_1$	$P6_422$ or $P6_222$
Unit-cell parameters (Å, °)	a = 54.66, b = 67.70, c = 85.30, $\alpha = \beta = \gamma = 90$	$a = b$ = 230.00, c = 114.47, $\alpha = \beta = 90$, $\gamma = 120$
Resolution (Å)	36.89–1.83 (1.90–1.83)	50–3.60 (4.25–4.16)
Measured reflections	3977702	365747
Unique reflections	48844	25957
Completeness (%)	99 (92)	96 (90)
Redundancy	80 (13)	27 (28)
Anomalous completeness (%)	92.5 (83.0)	N/A
No. of subunits in asymmetric unit	1	5 or 6
Phasing power	0.311 (0.069)	N/A
Figure of merit (centric/acentric)	0.08586/0.21770	N/A
$R_{\rm p.i.m.}$† (%)	0.80 (23.0)	N/A
$R_{\rm merge}$‡ (%)	8.5 (88.4)	9.6 (65.9)
$R_{\rm meas}$§ (%)	N/A	9.8 (67.0)
$\langle I/\sigma(I)\rangle$	40.2 (1.9)	31.7 (6.5)

† $R_{\rm p.i.m.} = \sum_{hkl}[1/(N-1)]^{1/2}\sum_i |I_i(hkl) - \langle I(hkl)\rangle|/\sum_{hkl}\sum_i I_i(hkl)$, where $I_i(hkl)$ and $\langle I(hkl)\rangle$ are the ith and the mean measurements of the intensity of reflection hkl and N is the redundancy. ‡ $R_{\rm merge} = \sum_{hkl}\sum_i |I_i(hkl) - \langle I(hkl)\rangle|/\sum_{hkl}\sum_i I_i(hkl)$. § $R_{\rm meas} = \sum_{hkl}[N/(N-1)]^{1/2}\sum_i |I_i(hkl) - \langle I(hkl)\rangle|/\sum_{hkl}\sum_i I_i(hkl)$.

rotating-anode generator equipped with a Platinum 135 CCD detector and a 300 µm collimator or the ID14-1 beamline at ESRF equipped with an ADSC Q210 CCD detector, using a beam size of 100 × 100 µm. Prior to cryocooling in a nitrogen stream, the form *A* crystals of $Mrs2_{16–276}$ were transferred into a cryoprotectant solution containing 30%(*v*/*v*) ethylene glycol, 56 m*M* sodium/potassium phosphate pH 6.3, while the form *B* crystals were transferred into a cryoprotectant solution containing 19% glycerol, 1.7 *M* NaCl, 70 m*M* imidazole pH 7.8. The form *A* crystals of $Mrs2_{16–276}$ diffracted to 1.83 Å resolution on an in-house source (Fig. 3*a*) and belonged to space group $P2_12_12_1$ (unit-cell parameters a = 54.66, b = 67.70, c = 85.30 Å), with the asymmetric unit containing one molecule. This is consistent with a Matthews coefficient of 2.32 Å^3 Da^{-1} and a solvent content of 47.0%. The form *B* crystals of $Mrs2_{16–276}$ diffracted to 4.16 Å resolution at ESRF (Fig. 3*b*) and belonged to space group $P6_222$ or $P6_422$ (unit-cell parameters $a = b$ = 230.00, c = 114.47 Å), with the asymmetric unit being likely to contain five or six molecules, corresponding to a Matthews coefficient of 2.84 Å^3 Da^{-1} and a solvent content of 56.7%.

The data-collection statistics are summarized in Table 1. Crystallographic data collected in-house were processed (integrated and scaled) with the *PROTEUM2* software suite (Bruker AXS Inc.), while the synchrotron data sets were processed using *XDS* (Kabsch, 2010).

2.5. Solution of the phase problem

The structure could not be solved by molecular replacement using the known CorA structure as a search model (Lunin *et al.*, 2006), but was instead solved by the single-wavelength anomalous dispersion method (SAD) using the Mrs2 native S atoms for phasing. A highly redundant (average multiplicity of 80) data set with high anomalous completeness (92.5%; 83.0% in the outermost shell) was obtained from a form *A* crystal using the in-house X-ray source with a 1.54 Å wavelength (Table 1). The diffraction data were cut to 2.5 Å resolution to determine the sulfur substructure using *SHELXD* (Sheldrick, 2008). All 11 S-atom sites were found, corresponding to the five cysteine and six methionine residues present in the protein. Subsequent heavy-atom refinement and density modification was performed using *autoSHARP* (Vonrhein *et al.*, 2007). The sulfur SAD phases obtained from *autoSHARP* produced an electron-density map which was traced using *ARP*/*wARP* (Morris *et al.*, 2003; Joosten *et al.*, 2008) and automatically fitted 243 of the 261 amino-acid residues in three different chains ($R_{\rm work}$ and $R_{\rm free}$ of 0.21 and 0.30, respectively) into the density. Structure determination is currently in progress using the diffraction data extending to 1.83 Å resolution.

We acknowledge the ESRF, Grenoble for provision of synchrotron radiation. MBK is the recipient of a PhD fellowship from FWF (P20141). This work was partially supported by WWTF (LS05021) and the University of Vienna.

References

Baumann, F., Neupert, W. & Herrmann, J. M. (2002). *J. Biol. Chem.* **277**, 21405–21413.
Bui, D. M., Gregan, J., Jarosch, E., Ragnini, A. & Schweyen, R. J. (1999). *J. Biol. Chem.* **274**, 20438–20443.
Diwan, J. J. (1987). *Biochim. Biophys. Acta*, **895**, 155–165.
Gardner, R. C. (2003). *Curr. Opin. Plant Biol.* **6**, 263–267.
Graschopf, A., Stadler, J. A., Hoellerer, M. K., Eder, S., Sieghardt, M., Kohlwein, S. D. & Schweyen, R. J. (2001). *J. Biol. Chem.* **276**, 16216–16222.
Ikari, A., Okude, C., Sawada, H., Yamazaki, Y., Sugatani, J. & Miwa, M. (2008). *Biochem. Biophys. Res. Commun.* **369**, 1129–1133.
Joosten, K., Cohen, S. X., Emsley, P., Mooij, W., Lamzin, V. S. & Perrakis, A. (2008). *Acta Cryst.* D**64**, 416–424.
Kabsch, W. (2010). *Acta Cryst.* D**66**, 125–132.
Knoop, V., Groth-Malonek, M., Gebert, M., Eifler, K. & Weyand, K. (2005). *Mol. Genet. Genomics*, **274**, 205–216.
Kolisek, M., Zsurka, G., Samaj, J., Weghuber, J., Schweyen, R. J. & Schweigel, M. (2003). *EMBO J.* **22**, 1235–1244.
Li, L., Tutone, A. F., Drummond, R. S., Gardner, R. C. & Luan, S. (2001). *Plant Cell*, **13**, 2761–2775.
Lunin, V. V., Dobrovetsky, E., Khutoreskaya, G., Zhang, R., Joachimiak, A., Doyle, D. A., Bochkarev, A., Maguire, M. E., Edwards, A. M. & Koth, C. M. (2006). *Nature (London)*, **440**, 833–837.
Mobasheri, A., Mobasheri, R., Francis, M. J., Trujillo, E., Alvarez de la Rosa, D. & Martin-Vasallo, P. (1998). *Histol. Histopathol.* **13**, 893–910.
Morris, R. J., Perrakis, A. & Lamzin, V. S. (2003). *Methods Enzymol.* **374**, 229–244.
Payandeh, J., Li, C., Ramjeesingh, M., Poduch, E., Bear, C. E. & Pai, E. F. (2008). *J. Biol. Chem.* **283**, 11721–11733.
Schmitz, C., Dorovkov, M. V., Zhao, X., Davenport, B. J., Ryazanov, A. G. & Perraud, A. L. (2005). *J. Biol. Chem.* **280**, 37763–37771.
Schock, I., Gregan, J., Steinhauser, S., Schweyen, R., Brennicke, A. & Knoop, V. (2000). *Plant J.* **24**, 489–501.
Sheldrick, G. M. (2008). *Acta Cryst.* A**64**, 112–122.
Voets, T., Nilius, B., Hoefs, S., van der Kemp, A. W., Droogmans, G., Bindels, R. J. & Hoenderop, J. G. (2004). *J. Biol. Chem.* **279**, 19–25.
Vonrhein, C., Blanc, E., Roversi, P. & Bricogne, G. (2007). *Methods Mol. Biol.* **364**, 215–230.
Wachek, M., Aichinger, M. C., Stadler, J. A., Schweyen, R. J. & Graschopf, A. (2006). *FEBS J.* **273**, 4236–4249.
Walker, G. M., Birchandersen, A., Hamburger, K. & Kramhoft, B. (1982). *Carlsberg Res. Commun.* **47**, 205–214.
Warren, M. A., Kucharski, L. M., Veenstra, A., Shi, L., Grulich, P. F. & Maguire, M. E. (2004). *J. Bacteriol.* **186**, 4605–4612.
Weghuber, J., Dieterich, F., Froschauer, E. M., Svidova, S. & Schweyen, R. J. (2006). *FEBS J.* **273**, 1198–1209.
Zsurka, G., Gregan, J. & Schweyen, R. J. (2001). *Genomics*, **72**, 158–168.